

A microscopic model for the structural transition and spin gap formation in α' - NaV_2O_5

A. Bernert¹, P. Thalmeier², P. Fulde¹

¹ *Max-Planck-Institut für Physik komplexer Systeme, D-01187 Dresden, Germany*

² *Max-Planck-Institut für Chemische Physik fester Stoffe, D-01187 Dresden, Germany*

(October 25, 2018)

Abstract

We present a microscopic model for α' - NaV_2O_5 . Using an extended Hubbard model for the vanadium layers we derive an effective low-energy model consisting of pseudospin Ising chains and Heisenberg chains coupled to each other. We find a “spin-Peierls-Ising” phase transition which causes charge ordering on every second ladder and superexchange alternation on the other ladders. This transition can be identified with the first transition of the two closeby transitions observed in experiment. Due to charge ordering the effective coupling between the lattice and the superexchange is enhanced. This is demonstrated within a Slater-Koster approximation. It leads to a second instability with superexchange alternation on the charge-ordered ladders due to an alternating shift of the O sites on the rungs of that ladder. We can explain within our model the observed spin gap, the anomalous BCS ratio, and the anomalous shift of the critical temperature of the first transition in a magnetic field. To test the calculated superstructure we determine the low-energy magnon dispersion and find agreement with experiment.

I. INTRODUCTION

The layered oxide α' - NaV_2O_5 has attracted great interest since 1996, when Isebe and Ueda reported a phase transition at $T = 34$ K with a spin-Peierls like spin gap formation [1]. At low temperatures the spin gap has a size of about $\Delta \approx 100$ K [1–3], which yields a BCS ratio $2\Delta/k_B T_C \approx 6$, much higher than for other organic or inorganic spin-Peierls materials, for which it lies around the canonical BCS-value of 3.5.

Furthermore, experiments have shown that there are actually *two* transitions, which lie very close to each other [4,5]. Both are of second order. The first one at $T_{C1} \approx 34$ K is accompanied by a logarithmic peak in the specific heat [6,7] while the second at $T_{C1} - T_{C2} \approx 0.3$ K is of mean-field character evident from a jump in the specific heat. NMR measurements suggest that the first transition leads to charge ordering while the second one opens a spin gap [5].

Measurements of the critical exponents yield $\beta_\delta \approx 0.15 \dots 0.2$ for the critical exponent of the lattice distortion δ and $\beta_\Delta \approx 0.34$ for the critical exponent of the spin gap Δ [8–11]. From these values the existence of two transition can also be inferred indirectly. Close to the critical point the spin gap Δ due to a lattice distortion δ is expected to obey $\Delta \propto \delta^{3/4}$ [12], corresponding to $\beta_\Delta = 3/4\beta_\delta$. This relation is not fulfilled in α' - NaV_2O_5 , indicating the existence of two separate transitions.

For $T > T_{C1}$ α' - NaV_2O_5 has equivalent V sites [13–15] implying valence 4.5+. For $T < T_{C2}$ ^{51}V -NMR measurements so far show only two inequivalent sites [16] while x-ray structure determination reports three inequivalent sites [17–19].

An interesting experimental observation is the magnetic field dependence of T_{C1} . It is only about 25% of the value expected for a spin-Peierls transition [4,20,21] but on the other hand, it is much higher than what would be generally expected for a structural transition [22].

In this article we explain a number of these above mentioned features by an analysis of a microscopic model. We find that the phase transition at T_{C1} can be regarded as a combination of charge-ordering on every second ladder and superexchange alternation on the other ladders, a “spin-Peierls-Ising” transition. This also explains the anomalous shift of T_{C1} in a magnetic field. The phase transition at T_{C2} can be regarded as a spin-Peierls transition on the charge-ordered ladders. It is driven by the charge ordering. The lattice distortion accompanying the charge ordering increases the coupling constant of a lattice mode invoking superexchange alternation on the charge-ordered ladders. With increasing charge ordering for decreasing temperatures the coupling constant increases until the second phase transition takes place at T_{C2} . This second phase transition opens a spin gap in agreement with experimental observations. Charge ordering is not yet complete at T_{C2} . The coupling constant therefore continues to increase and due to this the low-temperature spin gap is larger than what would be expected from T_{C2} , i.e., the BCS ratio is enhanced.

We test our low-temperature structure against x-ray structure determination and find it to agree within experimental resolution. Furthermore we calculate the low-energy magnon dispersion and find it to agree nicely with experimental results from inelastic neutron scattering [2,3].

This article is organised as follows. In the next section we consider a microscopic model which we project onto a spin-pseudospin model describing low-energy charge and spin degrees of freedom similar to [23–25]. We find that a “zig-zag” charge ordering as observed in

experiment requires the inclusion of spin and lattice degrees of freedom, not only the charge degrees of freedom. We therefore extend the spin-pseudospin Hamiltonian to include lattice degrees of freedom.

In section III we analyse this Hamiltonian using RPA. We find two phase transitions occurring one after the other, one being a combination of charge ordering and spin-dimerisation on different ladders, the other being a pure spin-Peierls transition.

In section IV we compare the calculated low temperature structure with experiment. As regards x-ray structure determination we argue that within experimental resolution theory and experiment agree. With the calculated low-temperature structure we explain the magnon dispersion observed in experiment. Finally we summarize and discuss our results.

II. DERIVATION OF THE MODEL HAMILTONIAN

To construct a model Hamiltonian we note that according to LDA+U calculations [26] the orbitals around the Fermi level are mostly of vanadium d_{xy} character. They are separated both from the lower lying oxygen p orbitals as well as from the remaining vanadium d -orbitals and the sodium 3s orbital which lie energetically higher. This means that we have to consider only the quarter filled d_{xy} orbitals. For a discussion of charge ordering we restrict ourselves to a 2D model neglecting hopping matrix elements and Coulomb interactions between the vanadium layers. The former have been shown to be negligible both by LDA+U [26] and Slater-Koster type calculations [19]. The Coulomb interactions are expected to be small due to the large distance between the V sites of neighbouring layers. They are also screened by intermediate O ions. Therefore our initial Hamiltonian represents an extended one-band Hubbard model at quarter filling, taking on-site and intersite Coulomb interactions into account:

$$\begin{aligned}
H = & \sum_{\langle\langle i,j \rangle\rangle_R} t_R \left(a_{i\sigma}^\dagger a_{j\sigma} + \text{h.c.} \right) + \sum_{\langle\langle i,j \rangle\rangle_L} t_L \left(a_{i\sigma}^\dagger a_{j\sigma} + \text{h.c.} \right) \\
& + \sum_{\langle i,j \rangle_{IL}} t_{IL} \left(a_{i\sigma}^\dagger a_{j\sigma} + \text{h.c.} \right) + \sum_{\langle\langle i,j \rangle\rangle_D} t_D \left(a_{i\sigma}^\dagger a_{j\sigma} + \text{h.c.} \right) \\
& + \sum_{\langle\langle i,j \rangle\rangle_R} V_R n_i n_j + \sum_{\langle\langle i,j \rangle\rangle_L} V_L n_i n_j \\
& + \sum_{\langle i,j \rangle_{IL}} V_{IL} n_i n_j + \sum_i U n_{i\uparrow} n_{i\downarrow}. \tag{1}
\end{aligned}$$

Here \langle, \rangle_{IL} denotes pairs of nearest neighbour vanadium d_{xy} -orbitals while $\langle\langle, \rangle\rangle_R$ and $\langle\langle, \rangle\rangle_L$ denote pairs of next nearest neighbour vanadium d_{xy} -orbitals along the rung (R) or the leg (L). The first four terms describe the effective hopping of the d -electrons between V sites i and j . This hopping can take place both via oxygen orbitals and sodium orbitals. The last four terms describe the intersite and on-site Coulomb repulsion. These terms connect sites as shown in Fig. 1.

At $T > T_{C1}$ the system is at quarter filling and the V sites are all equivalent [13]. Therefore there is an average of one electron per rung. The on-site [15,27] and the intersite Coulomb repulsion create a charge transfer gap, causing α' - NaV_2O_5 to be an insulator.

Therefore hopping between rungs takes place only virtually. This enables us to use an effective Hamilton operator \tilde{H}_{PP} which acts on the Hilbert subspace \mathcal{P} of all states with one electron on each rung. Let \mathcal{Q} be the Hilbert subspace complementary to \mathcal{P} and P be the projector onto \mathcal{P} and Q the projector onto \mathcal{Q} . An eigenstate $|\psi_{PP}^{(0)}\rangle$ of \tilde{H}_{PP} satisfies:

$$\begin{aligned}\tilde{H}_{PP}|\psi_{PP}^{(0)}\rangle &= (PHP - PHQ(QHQ - E_0)^{-1}QHP)|\psi_{PP}^{(0)}\rangle \\ &= E_0|\psi_{PP}^{(0)}\rangle.\end{aligned}\tag{2}$$

To calculate \tilde{H}_{PP} we need to know the energies E_0 which can be either determined self-consistently or, as for a Schrieffer-Wolff transformation, set equal to the eigenenergy E_0^{PP} of PHP . In the following we are interested in \tilde{H}_{PP} only to order $O(t^2/E)$, i.e., to second order in the hopping. In this case we can neglect the hopping terms in $(QHQ - E_0)$, since both PHQ and QHP scale with t .

Within the subspace \mathcal{P} we use the operators $a_{i\alpha\sigma}^\dagger, a_{i\alpha\sigma}$ for the electrons in the atomic orbitals. Here i denotes the rung, the pseudospin variable $\alpha = \pm\frac{1}{2}$ describes whether the electron occupies the left ($-\frac{1}{2}$) or right ($+\frac{1}{2}$) V site of a rung and σ denotes the z-component of the spin. Using these operators we define the conditional creation operators

$$\hat{a}_{i\alpha\sigma}^\dagger = (1 - n_{i\bar{\alpha}\uparrow})(1 - n_{i\bar{\alpha}\downarrow})(1 - n_{i\alpha\bar{\sigma}})a_{i\alpha\sigma}^\dagger$$

similar to the operators used in the t - J -model [28]. We then obtain for \tilde{H}_{PP} :

$$\begin{aligned}\tilde{H}_{PP} &= H_S + \sum_i 2\hat{t}_R^i T_i^x + \sum_{\langle i,j \rangle_{IL}} \hat{K}_{IL}^{ij} T_i^z T_j^z \\ &+ \sum_{\langle\langle i,j \rangle\rangle_L} \left(\hat{K}_{Lz}^{ij} T_i^z T_j^z + \hat{K}_{Lx}^{ij} T_i^x T_j^x + \hat{K}_{Ly}^{ij} T_i^y T_j^y \right)\end{aligned}\tag{3}$$

where the \hat{K} , H_S and \hat{t}_R contain spin operator products. It turns out to be useful to work with spin and pseudospin operators

$$\begin{aligned}\vec{S}_i &= \frac{1}{2} \sum_{\sigma_1, \sigma_2, \alpha} \hat{a}_{i\alpha\sigma_1}^\dagger \vec{\sigma}_{\sigma_1\sigma_2} \hat{a}_{i\alpha\sigma_2}, \\ \vec{T}_i &= \frac{1}{2} \sum_{\sigma, \alpha_1, \alpha_2} \hat{a}_{i\alpha_1\sigma}^\dagger \vec{\sigma}_{\alpha_1\alpha_2} \hat{a}_{i\alpha_2\sigma}.\end{aligned}$$

In equation (3) \vec{S}_i denotes the spin of the electron on the i -th rung and the z component of \vec{T}_i corresponds to α , so the pseudospin \vec{T}_i describes the hopping of the electron between the two V sites of a rung. Furthermore

$$\begin{aligned}
H_S &= \sum_{\langle i,j \rangle_L} \left(\frac{2t_D^2}{U + \Delta_D^U - E_0^{PPP}} + \frac{2t_L^2}{U + \Delta_L^U - E_0^{PPP}} \right) \left(\vec{S}_i \vec{S}_j - \frac{1}{4} \right) \\
\hat{t}_R^j &= t_R + \sum_{\langle i,j \rangle_L} t_L t_D \left(\frac{4\vec{S}_i \vec{S}_j - 1}{2(U + \Delta_{LD}^U - E_0^{PPP})} \right. \\
&\quad \left. + \frac{4\vec{S}_i \vec{S}_j - 1}{2(V_R + \Delta_{LD}^V - E_0^{PPP})} \right) \\
\hat{K}_{IL}^{ij} &= -V_{IL} - \frac{t_{IL}^2 (4\vec{S}_i \vec{S}_j - 1)}{U + \Delta_{IL}^U - E_0^{PPP}} - \frac{2t_{IL}^2}{V_R + \Delta_{IL}^V - E_0^{PPP}} \\
\hat{K}_{Lz}^{ij} &= 2V_L + \frac{2t_L^2 (4\vec{S}_i \vec{S}_j - 1)}{U + \Delta_L^U - E_0^{PPP}} - \frac{2t_D^2 (4\vec{S}_i \vec{S}_j - 1)}{U + \Delta_D^U - E_0^{PPP}} \\
&\quad + \frac{4t_L^2}{V_R + \Delta_L^V - E_0^{PPP}} - \frac{4t_D^2}{V_R + \Delta_D^V - E_0^{PPP}} \\
\hat{K}_{Lx}^{ij} &= \frac{2t_L^2 (4\vec{S}_i \vec{S}_j + 1)}{V_R + \Delta_L^V - E_0^{PPP}} + \frac{2t_D^2 (4\vec{S}_i \vec{S}_j + 1)}{V_R + \Delta_D^V - E_0^{PPP}} \\
\hat{K}_{Ly}^{ij} &= \frac{2t_L^2 (4\vec{S}_i \vec{S}_j + 1)}{V_R + \Delta_L^V - E_0^{PPP}} - \frac{2t_D^2 (4\vec{S}_i \vec{S}_j + 1)}{V_R + \Delta_D^V - E_0^{PPP}}.
\end{aligned} \tag{4}$$

Here Δ^V and Δ^U are additional energy differences due to the local change of occupation numbers with hoppings. \hat{K}_{Lz} and \hat{K}_{IL} describe the most important interactions between electrons on neighbouring V sites. They drive the system to local “zig-zag” type ordering or local “in-line” type ordering of the V 3d electrons. Assuming that we have locally complete “zig-zag” short-range “ordering” within a ladder and no correlations between ladders the Δ^V , Δ^U are given by

$$\begin{aligned}
\Delta_L^V &= V_L, & \Delta_D^V &= 0, & \Delta_{IL}^V &= 2V_L, \\
\Delta_{LD}^V &= 0, & \Delta_L^U &= -V_L, & \Delta_D^U &= 0, \\
\Delta_{IL}^U &= -V_{IL}, & \Delta_{LD}^U &= -V_L.
\end{aligned} \tag{5}$$

Assuming that we have local “in-line” “ordering”, they are equal to

$$\begin{aligned}
\Delta_L^V &= V_{IL} - V_L, & \Delta_D^V &= 2V_{IL} - 2V_L, \\
\Delta_{IL}^V &= V_{IL} - 2V_L, & \Delta_{LD}^V &= 0, \\
\Delta_L^U &= -2V_{IL}, & \Delta_D^U &= V_{IL}, \\
\Delta_{IL}^U &= -V_{IL}, & \Delta_{LD}^U &= 0.
\end{aligned} \tag{6}$$

We now make a mean-field approximation for the spin operator products contained in \hat{K} and \hat{t}_R . With this we obtain an effective pseudospin model for the charge degrees of freedom. $K = \langle \hat{K} \rangle$ and $\tilde{t}_R = \langle \hat{t}_R \rangle$ become effective pseudospin coupling constants. This approximation should be acceptable since the corrections of the pseudospin part due to spin-spin-interactions are moderate.

With this approximation \tilde{H}_{PP} becomes the Hamiltonian for a strongly anisotropic pseudospin Heisenberg model in an “external field” $2\tilde{t}_R$. We calculate the effective coefficients \tilde{t}_R , K_L , K_{IL} assuming that $\langle \vec{S}_i \vec{S}_{i+1} \rangle = -\frac{3}{4}$ along the ladders and $\langle \vec{S}_i \vec{S}_j \rangle = \frac{1}{4}$ between ladders. This assumption is based on the LDA+U results for the sign of the intra-ladder and inter-ladder exchange constants [26]. We use Δ^V , Δ^U from (5) for the case of local “zig-zag” “ordering” and set E_0^{PP} to be the ground-state energy for *PHP*. E_0^{PP} is then given by the expression for the ground-state energy of the Ising chain in a transverse field [29] represented by t_R :

$$E_0 = 2(2t_R) \frac{|1 - \lambda_0|}{\pi} E \left(2\sqrt{\frac{-\lambda_0}{(\lambda_0 - 1)^2}} \right) \quad (7)$$

with $\lambda_0 = V_L/2t_R$ and E the complete elliptic integral of second kind. From the energies calculated in [26] by LDA+U for different configurations one obtains

$$2V_L - V_{IL} = 0.027 \text{ eV}. \quad (8)$$

To find V_R we assume that it can be obtained from V_L by scaling by d^3 with the different distances d of the V sites. Using the values for the parameters from Ref. [19], i.e., $t_R = -0.172$ eV, $t_L = -0.049$ eV, $t_D = -0.062$ eV, $t_{IL} = 0.110$ eV, $V_L = 2t_R$ and $U = 4$ eV, we find

$$\begin{aligned} \tilde{t}_R &= -0.190 \text{ eV} \\ K_{IL} &= -0.677 \text{ eV} \\ K_{Lz} &= 0.679 \text{ eV} \\ K_{Lx} &= -0.027 \text{ eV} \\ K_{Ly} &= 0.011 \text{ eV}. \end{aligned} \quad (9)$$

K_{Lx} and K_{Ly} are smaller than the other parameters by more than one order of magnitude and will therefore be neglected. Thus our model consists of Ising interactions K_{Lz} , K_{IL} and a “transverse field” $2\tilde{t}_R$

$$H_1 = \sum_{\langle\langle i,j \rangle\rangle_L} K_{Lz} T_i^z T_j^z + \sum_{\langle i,j \rangle_{IL}} K_{IL} T_i^z T_j^z + \sum_i 2\tilde{t}_R T_i^x. \quad (10)$$

The resulting geometry is triangular, as can be seen in Fig. 2a. Note that the first term is antiferromagnetic and the second term is ferromagnetic, resulting in geometrical frustration for the first two terms of equation (9).

We first consider the case $\tilde{t}_R = 0$. For this case the relation between the absolute sizes of K_{Lz} and K_{IL} determines the behaviour of the system [30]. If $|K_{Lz}| < |K_{IL}|$ the system undergoes a phase transition at some finite temperature into a low-temperature “ferromagnetic” state of the pseudospins with 2D-long range order. This state corresponds to an “in-line”-ordering of the electrons, i.e., chains of V^{4+} and V^{5+} alternate along a-direction.

If $|K_{Lz}| > |K_{IL}|$ the system remains disordered at any finite temperature. At $T = 0$ it enters an antiferromagnetic state of the pseudospins with 1D-order along b-direction and no correlation between neighbouring ladders. This corresponds to a “zig-zag”-ordering of V^{4+}

and V^{5+} along the ladders. Thus the system is effectively one-dimensional, although there are correlations between next-nearest-neighbour ladders [31].

In α' - NaV_2O_5 , we have $|K_{Lz}| > |K_{IL}|$. Therefore there is no phase transition at finite temperatures within the model described by equation (10), provided that $\tilde{t}_R = 0$ as assumed here. This is consistent with our choice of Δ^V, Δ^U . This qualitative result remains true for other choices for the hopping integrals resulting in different K_{Lz}, K_{IL} , e.g. those obtained from LDA in [26]. For $\tilde{t}_R = 0$ the system is therefore close to a quantum critical point with a transition from 1D ordering in b-direction to 2D long range order [32].

Next we consider the case $\tilde{t}_R \neq 0$. We note that the total Hamiltonian H_1 does not imply a phase transition into an ordered state at any finite temperature. This is due to the fact that the first two terms of H_1 do not lead to a phase transition as argued above and that the nonzero transverse field suppresses ordering even more. This result remains qualitatively true if we include the K_{Lx} and K_{Ly} terms from (9) which also suppress ordering. It also remains true if we include a small interlayer Ising-like interaction. This demonstrates that the phase transitions observed in α' - NaV_2O_5 cannot be of a purely Coulombic origin: to understand what happens in this material at low temperatures we have to include at least the spin degrees of freedom beyond the mean-field approximation used above. Furthermore, we know from Raman spectroscopy that there is a strong coupling between the charge distribution on the V sites and the distortion of the system [33]. A change in the position of a V sites implies a change in the positions of the O site on the leg of the neighbouring ladder. The displacement of the O ions can in turn affect the effective superexchange interaction as observed from experimental data in [19].

Therefore we generalize the Hamiltonian from equation (3), such that it contains lattice degrees of freedom. Such a Hamiltonian has the following form:

$$\begin{aligned}
H_{ISSP} = & \sum_{i,j} \tilde{K}_{Lz}^{ij} T_{ij}^z T_{i+1j}^z + \sum_{i,j} 2\tilde{t}_R T_{ij}^x + \sum_{i,j} J_{ij} \vec{S}_{ij} \vec{S}_{i+1j} \\
& + g_{Is} \sum_{ij} T_{ij}^z \vec{e}_0 \vec{u}_{ij} + \sum_{q,j} \omega_{qj}^{VO} b_{VO,qj}^\dagger b_{VO,qj} \\
& + \sum_{q,j} \omega_{qj}^{Na} b_{Na,qj}^\dagger b_{Na,qj} + \sum_{q,j} \omega_{qj}^{OR} b_{OR,qj}^\dagger b_{OR,qj}. \tag{11}
\end{aligned}$$

Here i numbers the rungs on a ladder, i.e., it denotes the (pseudo)spin on a chain, j denotes the ladder/chain in the lattice and \vec{e}_0 is a unit vector. We have introduced phonon operators b_{qj}^\dagger, b_{qj} for the displacement of neighboring V and O ions (VO) and for the displacement of Na or rung O ions (O_R). \vec{u} and J_{ij} are given by

$$\begin{aligned}
J_{ij} = & \left(1 + \vec{u}_{i+\frac{1}{2},j}^{VO} \vec{\nabla}_{i+\frac{1}{2},j}^{VO} + \vec{u}_{i+\frac{1}{2},j}^{Na} \vec{\nabla}_{i+\frac{1}{2},j}^{Na} + \vec{u}_{i+\frac{1}{2},j}^{OR} \vec{\nabla}_{i+\frac{1}{2},j}^{OR} \right) \\
& \times J(T_{ij}^z, T_{i+1j}^z) \\
J(T_{ij}^z, T_{i+1j}^z) = & J_0^{ij} (1 + f(T_{ij}^z, T_{i+1j}^z)) \\
\vec{u}_{ij} = & \sum_{\lambda q} \frac{1}{(mN)^{1/2}} \exp(i\vec{q}\vec{R}_{ij}) Q_j(\lambda\vec{q}) \\
Q_j(\lambda\vec{q}) = & b_{qj}^\dagger + b_{qj}. \tag{12}
\end{aligned}$$

H_{ISSP} essentially describes a spin-Peierls model with additional coupling to a one-dimensional Ising chain in a transverse field. It has to take into account the following observations.

At $T = 0$ K there is no correlation between pseudospins of neighbouring ladders for the pure Ising interaction case. Regarding the Coulomb interactions we may therefore treat the ladders as independent, setting $K_{IL} = 0$. The pseudospin part of the Hamiltonian (3) for each ladder is then described by a one-dimensional Ising model in a transverse field yielding the first two terms of H_{ISSP} . The property that the Hamiltonian (10) describes a model close to a quantum critical point has to be included in H_{ISSP} . Therefore we have to use an effective value for K_{Lz} which is close to the value needed for quantum critical behaviour of the pseudospin Ising chains. This effective value \tilde{K}_{Lz} is not necessarily identical to the “true” value of this Coulombic coupling in the material.

The spin part of the system behaves like a one-dimensional system at high temperatures [1], i.e., we can use a one-dimensional Heisenberg model for each ladder to describe it. These terms are contained in the third term of H_{ISSP} . The magnon dispersion at low-temperatures in a-direction is much smaller than in b-direction [2,3], even though interladder spin-spin coupling has a significant value [26]. Close to the disordered phase, however, interladder coupling is reduced due to frustration: as far as interladder spin-spin-coupling is concerned the system consists of triangles with one large antiferromagnetic and two smaller ferromagnetic interactions.

On each ladder spin and pseudospin degrees of freedom are coupled. This coupling is incorporated into the effective pseudospin coupling K_{Lz} and the effective coupling constant J_{ij} for the superexchange along the ladder.

A shift of V and neighbouring O ions is assumed to cause an effective staggered field in z-direction for the pseudospins on one leg of a ladder described by the fourth term of H_{ISSP} . Such a shift also causes a change in the superexchange for the neighbouring leg of the neighbouring ladder (see Fig. 4) which has to be incorporated into the effective coupling constant J_{ij} .

As has been argued in [19], a shift of the Na ions in c direction alternating along the ladder direction will cause an alternation in the superexchange along the ladder. The same effect is obtained by an alternating shift of O ions on a rung in b-direction. Such terms are included in J_{ij} and their significance will be examined in section III C.

The last three terms of H_{ISSP} describe the energies of the important lattice modes.

The spin-Peierls coupling contained in the expression for J_{ij} in (12) is slightly different from the normal form since it is the shift of the intermediate O ions or Na ions instead of the V ions, which causes the superexchange dimerisation. For parameters we will use $\tilde{t}_R = -0.190$ eV and $J_0 = 0.045$ eV for the case without charge ordering and no distortion.

The effective superexchange along a ladder J_{ij} defined in (12) consists of three parts: J_0^{ij} denotes the original superexchange for the ladder without charge ordering or distortions.

The second part, $J_0^{ij} f(T_{ij}^z, T_{i+1j}^z)$ describes the influence of the charge ordering on the superexchange. From numerical calculations we know that homogenous charge ordering on a ladder j causes a drop of the effective superexchange which is quadratic in $\langle T_j^z \rangle$, as can be seen in Fig. 5. The parabolic form of the curve can be understood from noting that the spectral weight of pair states with two particles on the same rung or the same leg decreases with $1 - (1 + \delta_{CO})(1 - \delta_{CO}) = \delta_{CO}^2$. Analytic calculations show a similar

behaviour [34]. Therefore $J_0^{ij} f(T_{ij}^z, T_{i+1j}^z)$ is approximately proportional to $(T_j^z)^2$ and the square of the distortion accompanying the charge ordering. If we use the experimental value for the phonon frequencies this effect is already contained in the high-temperature values of the phonon dispersion ω_{qj} and the term $J_0^{ij} f(T_{ij}^z, T_{i+1j}^z)$ is omitted, essentially making a mean-field approximation with regard to the spin operator products for this expression.

Finally, there is the essential contribution

$$\left(1 + \vec{u}_{i+\frac{1}{2},j}^{VO} \vec{\nabla}_{i+\frac{1}{2},j}^{VO} + \vec{u}_{i+\frac{1}{2},j}^{Na} \vec{\nabla}_{i+\frac{1}{2},j}^{Na} + \vec{u}_{i+\frac{1}{2},j}^{OR} \vec{\nabla}_{i+\frac{1}{2},j}^{OR}\right) J_0^{ij} (1 + f(T_{ij}^z, T_{i+1j}^z))$$

to the superexchange. It describes the coupling between distortion, superexchange dimerisation and charge ordering. Here we use a mean-field approximation for the pseudospin operator products. The term causes a competition between the spin-Peierls order parameter and charge order parameter on a ladder. \tilde{K}_{Lz} will be fitted to properly describe the system. As argued above, we must use \tilde{K}_{Lz} instead of K_{Lz} in equation (11).

III. PHASE TRANSITIONS

In this section we analyse the Hamiltonian given by equation (11). We have two types of instabilities to consider based on the third and fourth term. The first type results from the fourth term of equation (11) which describes a coupling between local distortions and charge ordering. By distortion the system reduces the interaction energy. Due to elastic coupling this is also accompanied by an alternating exchange coupling on neighbouring ladders. The second type results from the third term in equation (11) which includes a coupling between lattice and spin degrees of freedom leading to an instability of a spin-Peierls type.

In the following subsection we separate the system into two sublattices and first treat each subsystem on its own. Using RPA we analyze in subsection IIIB the first type of instability accompanied by charge ordering and superexchange alternation. We fit the free parameters g_{Is} and \tilde{K}_{Lz} as to obtain the proper value of T_{C1} and the shift of T_{C1} in a magnetic field. By analyzing the ground-state energy of different ordered states we find that at low temperatures half the ladders are charge-ordered and on the remaining half there is superexchange alternation.

In subsection IIIC we examine the influence of charge ordering on the second type of instability. The distortions of the charge-ordered ladders change the coupling $\vec{u}_{i+\frac{1}{2},j}^{OR} \vec{\nabla}_{i+\frac{1}{2},j}^{OR} J_0^{ij}$ and therefore the spin-lattice interaction. It will be shown that this interaction increases and results in a second phase transition. As shown below, this explains the anomalous BCS ratio.

A. Separation of the subsystems

The Hamiltonian (11) describes a model consisting of two subsystems 1 and 2 shown in Fig. 2b. Both subsystems contain Ising pseudospin chains alternating with Heisenberg spin chains. The Ising pseudospin chains describe the charge distribution on a ladder, and the Heisenberg spin chains describe the spin on a neighbouring ladder. The degrees of freedom on each rung (ij) are characterised by a pseudospin \vec{T}_{ij} on rung (ij) which is contained in

one subsystem and a spin \vec{S}_{ij} contained in the other subsystem. The two subsystems 1 and 2 describe the complete spin-charge dynamics of the Hamiltonian (11).

Neighbouring chains of the same subsystem are coupled by the lattice dynamics. A change of the superexchange along a spin chain is obtained, e.g., by a displacement of an O ion on a leg. Via the elastic coupling this causes a displacement of the neighbouring V site (see Fig. 4). Such a local distortion changes the chemical environment and therefore the on-site energy of the vanadium d_{xy} -orbital. This change in energy corresponds to a longitudinal field for the pseudospin of that rung. We assume that this field h_T^z is proportional to the displacement d_V of the V site of that rung and write:

$$h_T^z = 2g_{Is}d_V. \quad (13)$$

The two subsystems are coupled due to the dependence of the coupling J_{ij} on the charge distributions $\langle T_{ij}^z \rangle$ and $\langle T_{i+1j}^z \rangle$. J_{ij} describes the coupling of spins \vec{S}_{ij} and \vec{S}_{i+1j} in one subsystem and this term is contained in one subsystem, while $\langle T_{ij}^z \rangle$ and $\langle T_{i+1j}^z \rangle$ are operators used in the description of the other subsystem. The coupling between the charge-ordering evidence by nonzero $\langle T_{ij}^z \rangle$ and $\langle T_{i+1j}^z \rangle$ and the superexchange coupling J_{ij} along the ladder is negative. With increasing charge ordering along a ladder the effective superexchange coupling J_{ij} decreases as shown in Fig. 5. This may change, though, if we include the effect of lattice distortions accompanying the charge ordering. We then have to deal with a combination of effects on J_{ij} as argued above.

We first consider equation (11) for each of the two subsystems separately and then discuss the combined ordered ground-state. We can make a Wigner-Jordan transformation of the spin operators of a subsystem to obtain spinless fermions describing the spin degrees of freedom. Let $k_F = \pi/2b$ be the Fermi momentum of these spinless fermions where b is the lattice constant in b direction.

For a single subsystem, e.g., subsystem 1, alternation of the superexchange J_{ij} along the Heisenberg chains can be obtained by shifting the Na ions alternately in c-direction or by shifting the O ions on the rungs in b-direction as shown in Fig. 3. Applying the result of Cross and Fisher [35] we arrive at renormalized phonon frequencies for $q = 2k_F$:

$$\begin{aligned} \tilde{\omega}_{2k_F,OR}^2 &= \omega_{2k_F,OR}^2 - 0.26 |2g_{OR}(2k_F)|^2 T^{-1}, \\ \tilde{\omega}_{2k_F,Na}^2 &= \omega_{2k_F,Na}^2 - 0.26 |g_{Na}(2k_F)|^2 T^{-1}. \end{aligned} \quad (14)$$

The coupling of a shift of the Na ion to a superexchange alternation is smaller by a factor of 2, because a shift of the Na site in c-direction affects the superexchange only on one two-rung cluster whereas a shift of the rung O site in b-direction affects the superexchange on two neighbouring two-rung clusters.

For a single subsystem, e.g., subsystem 1, there is also an instability towards superexchange alternation along the Heisenberg chains accompanied by charge ordering along the Ising chains. This corresponds to shifts induced by the lattice mode q_0 with $q_0 = 2k_F$ as shown in Fig. 4. Within this mode the V sites on the chains of the A ladder shift in c-direction. The direction of the shift alternates along the ladder, corresponding to a staggered longitudinal field for the pseudospins of subsystem 1. The leg O ions on the B ladders also shift in c-direction together with the neighbouring V sites of the A ladder. This causes an alternation of the superexchange along the B ladder, corresponding to an alternation

of J_{ij} along the Heisenberg spin chains of subsystem 1. Applying the results of Cross and Fisher and using RPA for the effect of the pseudospin-lattice coupling one obtains

$$\tilde{\omega}_{q_0}^2 = \omega_{q_0}^2 - 0.26 |g_{VO}(q_0)|^2 T^{-1} - 4g_{Is}^2 \chi_{q_0}(T) \quad (15)$$

where the last term describes the influence of the Ising chains. Here $\chi_q(T)$ is the susceptibility of the Ising chain due to a longitudinal field along z-direction. g_{VO} describes the coupling of a shift of the V sites on the superexchange of the neighbouring ladder via a shift of the O site.

B. The phase transition at T_{C1}

We know from experiment that the phase transition at T_{C1} in α' - NaV_2O_5 is accompanied by charge ordering [5]. We therefore first consider equation (15). We can take g for the q_0 mode in Fig. 4 directly from the results in [19]:

$$g_{q_0}^{VO} = \sqrt{\frac{\hbar}{m_V} \frac{\delta_J^{\text{exp}} J}{d_V}} = 7.884 \cdot 10^9 \text{ K s}^{-1/2} \quad (16)$$

with $d_V = 6.0768$ pm being the square root of the average of the squared shifts of the V sites on the A ladder, $\delta_J^{\text{exp}} = 0.26$ the exchange dimerisation for layer a, $J = 522$ K and m_V the V ion mass. We also need to obtain $\chi_q(T)$. While this is very difficult for general values of q , it is facilitated considerably when $q = q_0$. In this case the effective field for the pseudospins due to the lattice distortion is staggered in b-direction. The Ising chain has an antiferromagnetic coupling $K_{Lz} > 0$ along b-direction. Calculating $\chi_{q_0}(T)$ means therefore to calculate the susceptibility of an antiferromagnetic Ising chain in a transverse field for the application of an infinitesimal staggered longitudinal field. This is equivalent to calculating the susceptibility of a ferromagnetic Ising model in a transverse field for the application of an infinitesimal constant longitudinal field. This susceptibility can be expressed via the pseudospin correlation function $\rho(\lambda, T)$:

$$\chi_{q_0}(T) = \beta \lim_{N \rightarrow \infty} \frac{1}{N} \sum_{i,j=1}^N \rho_{|i-j|}^z(\lambda, T) \quad (17)$$

where $\rho_{|i-j|}^z(\lambda, T) = \langle T_i^z T_j^z \rangle(\lambda, T)$ and $\beta = 1/k_B T$ is the inverse temperature. $\lambda = \tilde{K}_{Lz}/4\tilde{t}_R$ is the ratio between the pseudospin interaction and the transverse field and determines the properties of the Ising chain. $\lambda = \infty$ corresponds to the Ising chain without a transverse field, $\lambda = 0$ to the paramagnetic limit.

For an Ising chain in a transverse field $\rho_n^z(\lambda, T)$ can be written in the form of a Toeplitz determinant [29]. For large n according to Szegő's Theorem [36] we have

$$\rho_n^z(\lambda, T) = \frac{1}{4} P(\lambda, T) G^n(\lambda, T) \quad (18)$$

where expressions for $P(\lambda, T)$ and $G(\lambda, T)$ are found in [37]. Some simple limits are given below. To obtain $\chi_{q_0}(T)$ we assume that the asymptotic expression (18) is correct for all n . With this assumption summation of the series (17) yields

$$\chi_{q_0, \lambda} = \frac{1}{4} \beta P(\lambda, T) \frac{1 + G(\lambda, T)}{1 - G(\lambda, T)}. \quad (19)$$

The approximation is expected to be correct close to the quantum critical point, i.e., close to $\lambda = 1$ at $T = 0$, since then the susceptibility and the correlation length diverge. However, we can obtain $P(\lambda, T)$ and $G(\lambda, T)$ for the case $\lambda = \infty$, i.e., the pure Ising chain, from Ref. [37] as

$$\begin{aligned} P_{\lambda=\infty} &= 1 \\ G_{\lambda=\infty} &= \tanh(\beta\tilde{t}_R\lambda). \end{aligned} \quad (20)$$

When $\lambda = 0$ we are in the paramagnetic regime and find

$$\begin{aligned} P_{\lambda=0} &= \frac{2}{2\beta\tilde{t}_R} (1 - \lambda^2)^{-3/4} = \frac{2}{2\beta\tilde{t}_R}, \\ G_{\lambda=0} &= \lambda (\tanh[\beta\tilde{t}_R(1 + \lambda)]) \exp\left((2\pi\beta\tilde{t}_R)^{-1/2} \exp(-\beta\tilde{t}_R(1 - \lambda)) \dots\right) \\ &= 0. \end{aligned} \quad (21)$$

With these expressions we can calculate $\chi_{q_0}(T)$ in the limits $\lambda = \infty, 0$ and find

$$\chi_{q_0, \lambda=\infty}(T) = \frac{\beta}{4} \exp\left(\frac{1}{2}\beta\tilde{K}_{Lz}\right) \quad (22)$$

and

$$\chi_{q_0, \lambda=0}(T) = \frac{1}{2(2\tilde{t}_R)} \tanh\left(\frac{1}{2}\beta(2\tilde{t}_R)\right). \quad (23)$$

Both expressions (22) and (23) are equal to the exact solution in these limits which implies that this $\chi_{q_0, \lambda}$ should be a reasonable approximation for all values of λ . We can therefore in principle calculate T_{C1} from equation (15) knowing g_{Is} , ω_{q_0} and λ by simply setting $\tilde{\omega}_{q_0} = 0$.

We can find ω_{q_0} from measurements of the elastic constants [38]. There a strong anomaly in the c_{66} mode of α' - NaV_2O_5 was observed at the phase transition temperature. This mode couples to a zig-zag like charge ordering and we therefore identify it with the q_0 mode of the present calculations. Using the high temperature value for the sound velocity $v_{66} = 4200$ m/s we estimate $\omega_{q_0} = \pi v_{66}/b = 279$ K, where $b = 3.611$ Å is the lattice constant in b-direction for the undistorted lattice.

When ω_{q_0} is known we obtain λ and g_{Is} by fitting them to $T_{C1} = 34$ K and to the experimental value of the shift of T_{C1} in a magnetic field. The latter is reduced from its standard spin-Peierls value [39] due to the Ising part of the transition. This is seen as follows. Considering only the spin-Peierls part of the transition, applying a magnetic field lowers the transition temperature $T_{C1}(H = 0)$ without a magnetic field to a value $T_{C1}^{H, SP}$. On the other hand, the Ising chain susceptibility $\chi_{q_0, \lambda}(T)$ increases with decreasing temperature. This causes an increase of the critical temperature from $T_{C1}^{H, SP}$ to the observed phase transition temperature $T_{C1}(H) > T_{C1}^{H, SP}$ in a magnetic field.

The expansion for T_{C1} in a magnetic field H for a pure spin-Peierls system is [39]:

$$\frac{T_{C1}(H) - T_{C1}(H = 0)}{T_{C1}(H = 0)} = -0.36 \left(\frac{\mu_B H}{k_B T_{C1}(H = 0)} \right)^2. \quad (24)$$

Due to the influence of the Ising part this expression is modified to

$$\begin{aligned}\frac{T_{C1}(H) - T_{C1}^H}{T_{C1}^{H,Is}(0)} &= -0.36 \left(\frac{\mu_B H}{k_B T_{C1}^{H,Is}(0)} \right)^2 \\ \frac{k_B T_{C1}^{H,Is}}{J}(0) &= 0.8 \frac{(g_{q_0}^{VO})^2}{\pi J \omega_{q_0, \text{eff}}^2(T_{C1}(H))}\end{aligned}\quad (25)$$

in the present case with

$$\omega_{q_0, \text{eff}}^2(T_{C1}(H)) = \omega_{q_0}^2 - 4g_{Is}^2 \chi_{q_0, \lambda}(T_{C1}(H)). \quad (26)$$

For small shifts this leads to

$$\frac{T_{C1}(H) - T_{C1}(0)}{T_{C1}(0)} = -\frac{0.36}{1 + T_{C1}(0) a(T_{C1}(0))} \left(\frac{\mu_B H}{k_B T_{C1}(0)} \right)^2 \quad (27)$$

with

$$a(T) = -\frac{4g_{Is}^2 \frac{d\chi_{q_0, \lambda}(T)}{dT}}{\omega_{q_0}^2 - 4g_{Is}^2 \chi_{q_0, \lambda}(T)}. \quad (28)$$

From the experimental result for the shift of $T_{C1} = 34$ K in a magnetic field in [4,21,20] we obtain $a(T_{C1}) \approx 0.086$ K⁻¹. Fitting g_{Is} and λ to these two values we obtain

$$\begin{aligned}\lambda &= 0.99850 \\ g_{Is} &= 1.688 \text{ K}/(\text{pm shift of V}).\end{aligned}\quad (29)$$

Note that this value for λ is close to the value for the ratio $K_{IL}/K_{Lz} \approx 0.997$ from equation (9). This indicates that geometrical frustration plays an important role. To see how stable the solution is towards a change of the parameters, we evaluate the dependence of T_{C1} on \tilde{K}_{Lz} , ω_{q_0} and g_{Is} :

$$\begin{aligned}\frac{\partial T_{C1}}{\partial \tilde{K}_{Lz}} &= 1.06, \\ \frac{\partial T_{C1}}{\partial \omega_{q_0}} &= -0.14, \\ \frac{\partial T_{C1}}{\partial g_{Is}} &= 12 \text{ pm}.\end{aligned}\quad (30)$$

T_{C1} is rather sensitive to small changes of \tilde{K}_{Lz} or λ . This sensitivity is due to the fact, that $(1 - \lambda) \ll 1$. It is much less and the stability therefore much improved compared to the result presented in [25], where $\lambda \approx 0.99986$ was suggested.

Next we include the coupling between the two subsystems. For this we will use the mean-field values for $\langle T_{ij}^z \rangle$, $\langle T_{i+1j}^z \rangle$. They are zero at T_{C1} and therefore the critical temperature T_{C1} remains unchanged in this approximation. But a mean-field approximation is not reliable close to the critical point of the transition where fluctuations must be taken into account. We therefore consider the zero temperature free energy of different ordered states. For this

we need the dependence of the superexchange J_0^{ij} along a ladder on the charge ordering order parameter $\langle T_j^z \rangle$ on the same ladder. This is approximately

$$J_{ij}^{\text{eff}} = J_0^{ij} \left(1 - 4 \langle T_j^z \rangle^2 \right) \quad (31)$$

where we neglect a small contribution to J_{ij}^{eff} from the diagonal hopping in the case of complete charge ordering on the ladder, i.e., for $\langle T_j^z \rangle = \frac{1}{2}$. As argued at the end of section II, J_{ij}^{eff} enters our equations in two places. First, it effectively changes ω_{q_0} through $J_0 f(T_{ij}^z, T_{i+1j}^z)$. Since we used ω_{q_0} from experiment, this effect is already included. Second, J_{ij}^{eff} modifies the energy gain resulting from the spin degrees of freedom due to distortions and it is this effect we have to consider now. Using the expression for the magnetic energy gain from Ref. [12] for the alternating Heisenberg chain we can write down the energy gain $dF(T=0)$ of the ground-state of the ordered system versus that of the ground-state of the disordered system. The dimerisation parameter of the Heisenberg chains $\delta_J^{(1),(2)}$ with $\delta_J^{(1),(2)} = g_{q_0}^{VO} Q_{1,2}/J$ from equation (16) is the order parameter for each of the two subsystems. $Q = d_V \sqrt{m_V/\hbar}$ is the canonical displacement. We find:

$$\begin{aligned} dF(T=0) = & b(Q_1^2 + Q_2^2) - E_{SP}(Q_1) (1 - 4 \langle T_2^z \rangle^2) \\ & - E_{SP}(Q_2) (1 - 4 \langle T_1^z \rangle^2) - 2g_{Is} (\langle T_1^z \rangle Q_1 + \langle T_2^z \rangle Q_2) \end{aligned} \quad (32)$$

with

$$\begin{aligned} b &= \frac{1}{2} \omega_{q_0}^2, \\ E_{SP}(Q_{1,2}) &= 0.3134J \left(\delta_J^{(1),(2)} \right)^{4/3}, \\ \langle T_{1,2}^z \rangle &= \frac{1}{2} (1 - \exp(-4\chi_{Is}(T=0) g_{Is} Q_{1,2})). \end{aligned} \quad (33)$$

Here we assumed that T^z approaches $\frac{1}{2}$ exponentially if a staggered parallel field $g_{Is}Q$ is applied. In equation (32) E_{SP} denotes the energy gain from the spin-Peierls distortions, while the terms proportional to g_{Is} denote the energy gain from charge ordering. The first term stands for the elastic energy of the distortion. Optimizing equation (32) in $\delta_J^{(1),(2)} \in [0, 1]$ we find a minimum at $\delta_J^{(1)} = 0.023$, $\delta_Q^{(2)} = 0$ or vice versa with $dF = -0.80$ K. Requiring $\delta_J^{(1)} = \delta_J^{(2)} = \delta_J$, i.e., the equivalence of the two subsystems we find $\delta_J = 0.009$ with $dF = -0.35$ K. We have plotted in Fig. 6 dF for $\delta_J^{(1)} = \delta_J^{(2)}$ and $\delta_J^{(2)} = 0$. In the previous calculations we used $\delta_J^{\text{exp}} = 0.26$ to obtain $g_{q_0}^{VO}$, so the first result is more consistent with our calculation than the second one and it also has the lower energy.

From the derivation of χ_{Is} we can obtain the bare correlation length along the Ising chains as

$$\xi_{Is}(T) = -\frac{1}{\ln G(T)}. \quad (34)$$

At T_{C1} we find that $\xi_{Is} \approx 183$ lattice constants. This large value of ξ_{Is} might offer an explanation for the strong dependence of T_{C1} on doping. By substituting Na with Ca or depleting the system of Na additional electrons/holes are introduced into the system. This

implies double/zero occupancy of rungs. They weaken correlations along the Ising chains. A rough estimate of the critical doping value at which the phase transition temperature T_{C1} is suppressed is $x_C \approx 0.5\%$. We obtain it by assuming $x_C \xi_{Is} \approx 1$. This value is in qualitative agreement with experiment. Substituting Na by Ca the transition disappears between 1% and 2.5% of Ca [40]. For hole doping due to Na deficiency the transition disappears between 2% and 3% deficiency [41].

C. The phase transition at T_{C2}

Next we consider the second phase transition observed. According to [5] this transition is of the Ginzburg-Landau type. It opens a spin gap and creates a local distortion at the Na sites as observed from the changes of the quadrupolar electric field tensor. Charge ordering at the V sites starts before this transition sets in [5]. For these reasons and in order to explain the observation of eight inequivalent Na sites in ^{23}Na -NMR [5,42] we suggested in [19] that the opening of the spin gap in the system is due to an alternating shift of the Na ions along the charge-ordered A ladders as shown in Fig. 3a. A second possibility is an alternating shift of the rung O ions on the A ladders as shown in Fig. 3b.

By using the hopping matrix elements obtained in [19] for the charge-ordered ladder in layer a we can calculate the effective superexchange J dependence on the charge ordering δ_{CO} on the same ladder. As we did for the undistorted ladders (see Fig. 5), the superexchange is defined by the singlet-triplet gap on a two-rung cluster. It is obtained via exact diagonalisation. We know from experiment [2] that $J \approx 440$ K in the low-temperature phase. This value of J corresponds to an incomplete charge ordering $\delta_{CO}^0 = \frac{1}{2}(n_+ - n_-) \approx 0.32$ on the A ladders in agreement with experiment [5].

The hopping matrix elements t_L , t_D , t_R change due to the distortion accompanying the charge ordering [19]. We parametrize these changes with $t(\delta_{CO} = 0) - t(\delta_{CO}) \propto \delta_{lat} \propto \delta_{CO}$, and normalize the prefactors such that the hopping matrix elements from Ref. [19] for the high temperature undistorted ladder are obtained at $\delta_{CO} = 0$ and those for the charge ordered ladder are obtained at $\delta_{CO} = \delta_{CO}^0$.

Due to alternating shifts of the rung O ions or the Na ions, the effective hopping along the leg t_L and the effective diagonal hopping t_D alternate also. The size of this is given by the parameter $\delta_{t_{L,D}} = (t_+^{L,D} - t_-^{L,D}) / (t_+^{L,D} + t_-^{L,D})$. If we know δ_{t_L} and δ_{t_D} we can find the superexchange alternation parameter δ_J by calculating the superexchange for the inequivalent two-rung clusters [19]. This gives us an approximate value for the spin-lattice coupling. Using it, the parametrized t_L , t_D and t_R from above, and equation (14) for the critical temperature we find $T_{SP}(\delta_{CO})$ for a spin-Peierls transition depending on the charge ordering:

$$\frac{k_B T_{SP}(\delta_{CO})}{J(\delta_{CO})} = 0.8 \frac{4g_{Ox}^2(\delta_{CO})}{\pi J(\delta_{CO}) \omega_{Ox}^2}. \quad (35)$$

We can estimate the value ω_{Ox} from the velocity v_{22} of the c_{22} mode in [38]. It describes a longitudinal mode along b-direction as required for the proposed shifts of the rung O ions with $v_{22} = 6500$ m/s which yields $\omega_{Ox} = 432$ K. For given values of δ_{t_L} and δ_{t_D} we obtain the dependence of the critical temperature T_{SP} on the charge ordering δ_{CO} as shown in Fig. 7.

In the low-temperature limit the spin gap is approximately given by $\Delta(\delta_{CO}^0) \approx 1.8T_{SP}(\delta_{CO}^0)$. Therefore the BCS ratio is enhanced by a factor of $T_{SP}(\delta_{CO}^0)/T_{C1}$.

We search for values of δ_{t_L} and δ_{t_D} for which the following conditions are fulfilled: (i) without charge ordering the critical temperature for such a transition is below 34 K, since the spin gap opens only below the charge ordering temperature; (ii) with increasing charge ordering the critical temperature is required to increase, because an enhanced BCS ratio has been observed; (iii) at $\delta_{CO} = \delta_{CO}^0$ the spin gap $\Delta(\delta_{CO}) \approx 1.8T_C^{SP}(\delta_{CO}^0)$ should be approximately 100 K as found experimentally.

The result is found in Fig. 7. The conditions (i) to (iii) are fulfilled for $\delta_{t_L} = -0.059$, $\delta_{t_D} = 0.090$ and with $T_{C1} = 34$ K an effective BCS ratio of 6.05 is found. We therefore have a spin-Peierls phase transition which is driven by charge ordering on the same ladder. When the first transition takes place at about $T_{C1} = 34$ K charge ordering sets in on the A ladders. This changes the two-particle correlation functions and the effective hoppings so that T_{SP} increases as compared with its value without charge ordering. At some temperature $T_{C2} < T_{C1}$ we have $T_{SP}(\delta_{CO}(T_{C2})) = T_{C2}$ and a spin-Peierls transition driven by charge ordering takes place. This is caused by an alternating shift of the O ions on the rungs of the A ladders, probably together with a small alternating shift of the Na ions along the A ladders. This also causes an inequivalence of the Na sites along the A ladders, such that we have 8 inequivalent Na sites as observed in experiment [42]. Since this happens before δ_{CO} attains its final value, the spin gap at lower temperatures is larger than what would be expected from the standard BCS ratio and T_{C1} .

In order to see whether the values for δ_{t_L} and δ_{t_D} are plausible, we have investigated the effects of alternating shifts of the rung O or the Na sites on the effective hopping matrix elements between V sites on the ladders. For this we use the Slater-Koster method as described in [19]. The results are given in Table I. Those for δ_{t_L} and δ_{t_D} have been obtained for otherwise undistorted ladders. δ_{t_L} and δ_{t_D} are found to have opposite signs, as assumed above. This can be understood by noticing that an increase of diagonal hopping due to increased hopping via the Na sites goes together with a decrease of the hopping along the legs of the ladder. The effects of charge ordering distortions and of the shifts of Na or rung O sites on the hopping matrix elements are small. Therefore we may neglect higher-order effects resulting from combinations of the distortions.

The results in the first three rows of Table I are based on [19] where we included V-O, V-V and Na-O hopping matrix elements in the initial Hamiltonian, projecting these on effective V-V hopping matrix elements. However, it has been argued in [26] that direct hopping between the O sites should also contribute to the effective Hamiltonian. It remains unclear, which fraction of the total O-O hopping matrix elements obtained in [26] results from direct hopping and which fraction comes from indirect hopping via the neighbouring Na site. To investigate the effect of such a hopping on the shifts of the rung O ions we introduced O-O hopping matrix elements according to the Slater-Koster approximation for into the initial Hamiltonian and calculated effective V-V hopping matrix elements as before. One finds $t_R = -0.17$ eV, $t_L = 0.17$ eV, $t_D = -0.04$ eV, $t_{IL} = -0.16$ eV. Introducing an alternating shift of the rung O ions in b-direction by 1 pm leads to $\delta_{t_L} \approx 0.003$ and $\delta_{t_D} \approx 0.1$ as given in the fourth row of Table I. The effect especially on the diagonal hopping is much stronger than it is without inclusion of the direct O-O hopping matrix elements. However, these values for t_L and t_{IL} are far from those found by LDA [26] and ab-initio methods [43].

One can therefore conclude that at least within the Slater-Koster method the contribution of the direct O-O hopping should be small as expected for next-nearest neighbour hopping, although it may help to explain the small differences between the LDA results of [26] and our results in [19]. The results from Table I can serve only as an estimate of the values of the spin-lattice coupling.

IV. COMPARISON WITH X-RAY DIFFRACTION AND NEUTRON SCATTERING EXPERIMENTS

In the following we compare our results with experimental observations. We do this with respect to two types of experiment: x-ray structure determination [17–19] and inelastic neutron scattering results for the magnon dispersion [2,3]. We compute the latter for the calculated structure by using a local-dimer approximation.

Comparing our results with x-ray structure determination we find good agreement. In both cases we have a superstructure consisting of two inequivalent ladder types alternating along a -direction: charge-ordered A ladders and strongly dimerised B ladders. A phase with two A ladders separated by a B ladder is also correctly found. We can explain these findings with the analysis given in section III B: the displacement of the V sites on the A ladders and of the O sites on the B ladders cause a combined charge-ordering-spin-Peierls transition.

X-ray structure analysis finds $Fmm2$ symmetry in the low-temperature phase. In our model this symmetry is realized for $T_{C1} > T > T_{C2}$. However, the phase transition at T_{C2} obtained for our model in section III C is accompanied by a breaking of this symmetry. It results from the shift of the rung O ions on the A ladders, as shown in Fig. 3b. A low-temperature spin gap of $\Delta \approx 100$ K on these ladders requires a superexchange dimerisation of about 0.05 when $\Delta = 2J\delta_j^{3/4}$ from Ref. [12] is used with the experimental value for $J = 440$ K. The coupling constant at $\delta_{CO}^0 = 0.32$ is approximately 0.043 per pm shift of the rung O ion. This corresponds to an actual shift of 1.1 pm of each rung O ion on ladder A.

The intensity of the x-ray scattering for small scattering angles is proportional to Z^2 where Z is the ionic charge. Below T_{C2} only one O ion per two formula units shifts its position to break the $Fmm2$ symmetry. In addition as estimated above these displacements are smaller than the displacements caused by the phase transition at T_{C1} and below, where a displacement of 7.46 pm and 4.26 pm for the V sites on the A ladder is found experimentally. It is therefore well possible that the scattering peaks resulting from the lower symmetry cannot be observed within experimental resolution. Insofar x-ray structure determination results do not contradict our theoretical results for the second transition.

Magnon dispersion, however, should be greatly affected by a dimerisation. The structure which is obtained after the two transitions have taken place is schematically shown in Fig. 8. The calculated magnon dispersion for this structure should therefore be a good test of the theory. For other suggested structures it was found that the corresponding magnon dispersion disagrees with experimental results: in the case of a lattice with “zig-zag” charge order on all ladders, the dispersion along a -direction does not agree with experiments [44]. For the spin-cluster model proposed in [18] the magnon dispersions, both in a - and b -direction, do not agree with experiments either [45–47].

We therefore calculate the magnon dispersion at a temperature well below T_{C2} . In order to do this we use the spin-dimer representation following Refs. [44,48,49]. The initial

magnetic Hamiltonian is then

$$\begin{aligned}
H = & \sum_{i \in A} J_A \left(1 + (-1)^j \delta_A \right) \vec{S}_{ij} \vec{S}_{ij+1} \\
& + \sum_{i \in B} J_B \left(1 + (-1)^j \delta_B \right) \vec{S}_{ij} \vec{S}_{ij+1} \\
& + \sum_{\langle ij, mn \rangle} J_{IL}^{ij, mn} \vec{S}_{ij} \vec{S}_{mn}
\end{aligned} \tag{36}$$

for a geometry and $J_{IL}^{ij, mn}$ as shown in Fig. 8. It describes the pure spin part of equation (11) with the effects of lattice distortions and pseudospins included within the effective coupling constants. The large value of $\delta_B \approx 0.26$ at $T = 15$ K found in [19] corresponds to a large gap in the excitation spectrum of the B ladders. Using $\Delta_B = 2J_B \delta_B^{3/4}$ for the spin gap [12] and $J_B = 52$ meV from Ref. [19] we find $\Delta_B \approx 38$ meV. The B ladders should therefore not contribute directly to the low-lying parts of the magnon dispersion. Since we are only interested in these, we assume that we have an indirect exchange coupling between A ladders through the virtual singlet-triplet excitations of the B ladders. This results in an effective Hamiltonian:

$$\begin{aligned}
H = & \sum_{ij\gamma} J_A \left(1 + (-1)^j \delta_A \right) \vec{S}_{ij\gamma} \vec{S}_{ij+1\gamma} + \sum_{ij\gamma} J_a \vec{S}_{ij\gamma} \vec{S}_{i+1j\gamma} \\
& + \sum_{ij\gamma} J_D \vec{S}_{ij\gamma} \left(\vec{S}_{i+1j+1\gamma} + \vec{S}_{i+1j-1\gamma} \right) \\
& + \sum_{ij\gamma} J_c \vec{S}_{ij\gamma} \vec{S}_{ij\bar{\gamma}}
\end{aligned} \tag{37}$$

with corresponding geometry and couplings as shown in Fig. 9. This exchange Hamiltonian exhibits manifestly a doubling of the period along the a axis. Here we also introduced a superexchange J_c in c-direction between layers; it is assumed to exist mainly between the V_{21} sites which lie directly above each other [19]. We therefore have $\gamma = \pm 1$: Along c-direction the V sites of the A ladder are ordered as $\dots -V_{21} - V_{21} - V_{22} - V_{22} - \dots$ as shown in Fig. 10 [17–19]. Next we introduce dimer variables. We denote each dimer within the A ladder (see Fig. 9) by coordinates $ij\gamma$, which are not identical with the former coordinates of the spins. As denoted in Fig. 9 we then have spins $\vec{S}_{ij\gamma 1,2}$. The dimer variables are then:

$$\begin{aligned}
\vec{K}_{ij\gamma} &= \vec{S}_{ij\gamma 1} + \vec{S}_{ij\gamma 2} \\
\vec{L}_{ij\gamma} &= \vec{S}_{ij\gamma 1} - \vec{S}_{ij\gamma 2}.
\end{aligned} \tag{38}$$

With those, equation (37) takes the form

$$\begin{aligned}
H = & \frac{1}{4} J_A (1 + \delta_A) \sum_{ij\gamma} \vec{K}_{ij\gamma} \vec{K}_{ij\gamma} - \vec{L}_{ij\gamma} \vec{L}_{ij\gamma} \\
& + \frac{1}{4} J_A (1 - \delta_A) \sum_{ij\gamma} \vec{K}_{ij\gamma} \vec{K}_{ij+1\gamma} - \vec{L}_{ij\gamma} \vec{L}_{ij+1\gamma} \\
& + \frac{1}{4} J_a \sum_{ij\gamma} \vec{K}_{ij\gamma} \vec{K}_{i+1j\gamma} - \vec{L}_{ij\gamma} \vec{L}_{i+1j\gamma} \\
& + \frac{1}{4} J_D \sum_{ij\gamma} \left(\vec{K}_{ij\gamma} - \vec{L}_{ij\gamma} \right) \left(\vec{K}_{i+1j\gamma} - \vec{L}_{i+1j\gamma} \right. \\
& \quad \left. + \vec{K}_{i+1j+1\gamma} - \vec{L}_{i+1j+1\gamma} \right) + \left(\vec{K}_{ij\gamma} + \vec{L}_{ij\gamma} \right) \\
& \quad \times \left(\vec{K}_{i+1j\gamma} + \vec{L}_{i+1j\gamma} + \vec{K}_{i+1j+1\gamma} + \vec{L}_{i+1j+1\gamma} \right) \\
& + \frac{1}{2} J_c \sum_{ij\gamma} \vec{K}_{ij\gamma} \vec{K}_{ij\bar{\gamma}} + \vec{L}_{ij\gamma} \vec{L}_{ij\bar{\gamma}}. \tag{39}
\end{aligned}$$

As in Ref. [44] we will only use the products $L_{ij\gamma} L_{mn\gamma'}$, since the other terms do not contribute to the dispersion of the spin excitations. We then transform the \vec{L} to

$$\begin{aligned}
\vec{L}_{ij\gamma} &= \frac{1}{\sqrt{2}} \left(\vec{M}_{ij}^+ + \vec{M}_{ij}^- \right) \\
\vec{L}_{ij\bar{\gamma}} &= \frac{1}{\sqrt{2}} \left(\vec{M}_{ij}^+ - \vec{M}_{ij}^- \right). \tag{40}
\end{aligned}$$

Furthermore we assume that the ladder designated by $(i+1, \gamma)$ is equivalent to the ladder $(i, \bar{\gamma})$. This corresponds to a geometry of the A ladders shown in Fig. 10. We therefore set $L_{ij\gamma} = L_{i+1j\bar{\gamma}}$, and separate the Hamiltonian into two parts:

$$\begin{aligned}
H_{M^+} = & -\frac{1}{4} (J_A (1 + \delta_A) - J_c) \vec{M}_{ij}^+ \vec{M}_{ij}^+ \\
& - \frac{1}{4} J_A (1 - \delta_A) \vec{M}_{ij}^+ \vec{M}_{ij+1}^+ - \frac{1}{4} J_a \vec{M}_{ij}^+ \vec{M}_{i+1j}^+ \\
& + \frac{1}{2} J_D \left(\vec{M}_{ij}^+ \vec{M}_{i+1j}^+ + \vec{M}_{ij}^+ \vec{M}_{i+1j+1}^+ \right), \\
H_{M^-} = & -\frac{1}{4} (J_A (1 + \delta_A) + J_c) \vec{M}_{ij}^- \vec{M}_{ij}^- \\
& - \frac{1}{4} J_A (1 - \delta_A) \vec{M}_{ij}^- \vec{M}_{ij+1}^- + \frac{1}{4} J_a \vec{M}_{ij}^- \vec{M}_{i+1j}^- \\
& - \frac{1}{2} J_D \left(\vec{M}_{ij}^- \vec{M}_{i+1j}^- + \vec{M}_{ij}^- \vec{M}_{i+1j+1}^- \right). \tag{41}
\end{aligned}$$

The first term of each Hamiltonian describes an effective dimer with interaction strength $J_A (1 + \delta_A) \pm J_c$. Its dynamical susceptibility is

$$u_{\alpha\beta}^{\pm}(\omega) = \delta_{\alpha\beta} (\delta_{\alpha x} + \delta_{\alpha y}) \frac{2 (J_A (1 + \delta_A) \mp J_c)}{(J_A (1 + \delta_A) \mp J_c)^2 - \omega^2}. \tag{42}$$

The dynamical RPA susceptibility of coupled dimers without anisotropy of the superexchange is given by

$$\chi(\vec{q}, \omega) = [1 - J(\vec{q}) u_{xx}(\omega)]^{-1} u_{xx}(\omega) \tag{43}$$

where J is the exchange term between dimers as given by the last four terms of H_{M+} and H_{M-} . After Fourier transformation these, J^+ for H_{M+} and J^- for H_{M-} are given by

$$J^\pm(\vec{q}) = \frac{1}{2}J_A(1 - \delta_A)\cos 2k_y \pm \left(\frac{1}{2}J_a\cos(k_x - k_y) - 2J_D\cos k_x\cos k_y \right). \quad (44)$$

Here $k_x = 2\pi q_x/a$, $k_y = 2\pi q_y/b$ with a and b being the lattice constants of the high temperature unit cell. We note a doubling of the unit cell in b -direction as required before by equation (37). The spin-wave excitations are obtained from the poles of $\chi(\vec{q}, \omega)$. With equations (42) and (44) we obtain

$$\omega_\pm^2 = (J_A(1 + \delta_A) \mp J_c)^2 - (J_A(1 + \delta_A) \mp J_c) \times (J_A(1 - \delta_A)\cos 2k_y \pm (J_a\cos(k_x - k_y) - 4J_D\cos k_x\cos k_y)). \quad (45)$$

We set $J_a^{\text{eff}} = J_a - 4J_D$ and $J_A = 440$ K, as used in our previous analysis and obtained from experiment [2]. Then we fit the unknown parameters J_a^{eff} , J_c and δ_A to the experimental values for three of the four gaps obtained from ω_+ and ω_- . These gap values have been observed for $T \leq 4.2$ K at $q_x = 0$, $q_y = \frac{1}{2}$ and $q_x = 0$, $q_y = 1$ [3]. Fitting three of the four gaps of sizes 10.9 meV, 10.1 meV, and 9.1 meV we obtain

$$\begin{aligned} J_a^{\text{eff}} &= 0.212 \text{ meV}, \\ J_c &= 0.431 \text{ meV}, \\ \delta_A &= 0.0310. \end{aligned} \quad (46)$$

This determines the fourth gap to be 8.14 meV which is in excellent agreement with the experimental value 8.2 meV from Ref. [3]. In the model presented here these spin gaps result from the assumed dimerisation of the charge ordered A ladders whereas previously the origin of the spin gaps was suggested to lie in an anisotropy of the superexchange [44]. The dispersion of ω^\pm along a -direction for $q_y = \frac{1}{2}, 1$ are shown in Fig. 11. These curves also agree with experiments.

The low value of J_a^{eff} , which causes the dispersion along a -direction is due to an effective coupling of next-nearest-neighbour ladders. Furthermore, J_a is partly compensated due to J_D couplings.

The value for J_c , which causes the gap between the two modes, corresponds to a hopping $t_c \approx 0.021$ eV between neighbouring V sites of neighbouring layers when $J_c = \frac{4t_c^2}{U}$ and $U = 4$ eV are used. This is in reasonable agreement with the value $t_c = 0.015$ eV found in [19] from the low-temperature structural data by a Slater-Koster approximation.

We can also obtain the approximate dispersion in b -direction for $q_x = 0$ as shown in Fig. 12. The maximum is at $\omega \approx 55$ meV and agrees nicely with the value $\omega_{max} = 59.5$ meV estimated in [2] from experimental data.

We therefore conclude that the results of our analysis in section III agree well with both the experimental results of x-ray structure determination and the magnon dispersion found by inelastic neutron scattering results for the magnon dispersion.

V. SUMMARY AND CONCLUSIONS

In this article we provided a theoretical description of the phase transitions in α' - NaV_2O_5 . In section II we started from a single band extended Hubbard model describing the hopping of electrons between V sites. We projected this model onto an effective spin-pseudospin Hamiltonian similar to that in Refs. [23–25]. Using parameters obtained from a previous Slater-Koster analysis and findings of LDA+U we argued that within the given model a phase transition cannot occur from Coulomb interactions only: the effective lattice for such a transition is triangular and its geometric frustration suppresses charge order, a distinctive feature which is present in the observed transition. We therefore constructed a minimal microscopic model based on a spin-pseudospin Hamiltonian which incorporates the coupling between charges, spins and the lattice.

In section III we analyzed this model with regard to phase transitions. We divided the model into two subsystems. Each of it describes the charge degrees of freedom on the rungs of half the ladders and the spin degrees of freedom on the other ladders. For each subsystem we find an instability towards a transition at T_{C1} which causes “zig-zag” charge ordering and superexchange dimerisation. With this combined spin-Peierls-Ising transition we can explain the anomalous shift of T_{C1} in a magnetic field. It is reduced from its normal spin-Peierls value due to the influence of the charge ordering. By calculating the free energy at $T = 0$ we found that the system should enter a phase where half of the ladders are “zig-zag” charge-ordered (A ladders), while the other half (B ladders) shows a strong superexchange alternation. The reason for this asymmetry lies in a competition between the order parameters for charge ordering and superexchange dimerisation due to a shift of the leg O sites on the same ladder. This explains observations of x-ray structure determination. Due to the strong effect of the one-dimensional Ising chains we can also explain qualitatively the strong dependence of the transition on depletion of Na or substitution of Na with Ca.

By analyzing the coupling between superexchange dimerisation and lattice distortion in the charge-ordered ladders we found that another transition is induced. Charge ordering increases the coupling between an alternating shift of the O sites on a rung and the superexchange alternation beyond the threshold value of a second transition at T_{C2} . The system then enters a phase where the charge-ordered A ladders dimerise and a spin gap opens. Due to the alternation the Na sites along the A ladders become inequivalent, such that we have 8 inequivalent Na sites as observed in ^{23}Na -NMR [5,42], not only 6 as would be the case in the $Fmm2$ symmetry indicated by x-ray structure determination.

This also helps to explain the discrepancy between measurements of the critical exponent of the lattice distortion [9–11] and of the critical exponent of the spin gap opening [8]: the former is smaller than the latter whereas one would expect the opposite for a single transition due to $\Delta \propto \delta_{lat}^{3/4}$. From the observations of a logarithmic peak in the specific heat at T_{C1} and the observation of fluctuations by x-ray diffuse scattering [11] we conclude that the transition at T_{C1} is mainly of 2D Ising character whereas the second transition at T_{C2} , which opens the spin gap, can be described within a mean-field theory. Since the charge ordering is not complete, when the second phase transition is triggered, the coupling constant further increases for decreasing temperatures. This leads to an additional increase of the spin gap and also of the BCS ratio. The conventional BCS ratio does not account for the temperature dependence of the coupling constant $g_{q_0}^{VO}$.

Within experimental resolution we find agreement with the x-ray structure determination. The second transition breaking the $Fmm2$ symmetry comprises only a small shift of every tenth O site. We also find excellent agreement with experimental results for the magnon dispersion at a temperature well below T_{C2} .

In conclusion we presented a microscopic model for α' - NaV_2O_5 which yields two phase transitions close to each other. The first is a “spin-Peierls-Ising” transition causing charge order and superexchange dimerisation. The second is a pure spin-Peierls transition triggered by an increase of the coupling constant due to charge ordering. With this model we can explain qualitatively and quantitatively a number of experimental observations, i.e., the existence of two transitions, the general structure of the low-temperature phase, the anomalous shift of T_{C1} in a magnetic field, the anomalous BCS ratio, the strong dependence of the transition on doping, and the observed low-energy magnon dispersion.

REFERENCES

- [1] M. Isobe and Y. Ueda, *J. Phys. Soc. Jpn.* **65**, 1178 (1996).
- [2] T. Yosihama, M. Nishi, K. Nakajima, K. Kakurai, Y. Fujii, M. Isobe, C. Kagami, and Y. Ueda, *J. Phys. Soc. Jpn.* **67**, 744 (1998).
- [3] B. Grenier, L. Regnault, J. Lorenzo, T. Ziman, J. Boucher, A. Hiess, T. Chatterji, J. Jegoudez, and A. Revcolevschi, *cond-mat/0007025* (2000).
- [4] M. Köppen, D. Pankert, R. Hauptmann, M. Lang, M. Weiden, C. Geibel, and F. Steglich, *Phys. Rev. B* **57**, 8466 (1998).
- [5] Y. Fagot-Revurat, M. Mehring, and R. Kremer, *Phys. Rev. Lett.* **84**, 4176 (2000).
- [6] D. Powell, J. Brill, Z. Zeng, and M. Greenblatt, *Phys. Rev. B* **58**, R2937 (1998).
- [7] M. Dischner, private communication.
- [8] P. Fertey, M. Poirier, M. Castonguay, J. Jegoudez, and A. Revcolevschi, *Phys. Rev. B* **57**, 13698 (1998).
- [9] S. Ravy, J. Jegoudez, and A. Revcolevschi, *Phys. Rev. B* **59**, R681 (1999).
- [10] H. Nakao, K. Ohwada, N. Takesue, Y. Fujii, M. Isobe, and Y. Ueda, *J. Phys. Chem. Solids* **60**, 1101 (1999).
- [11] B. Gaulin, M. Lumsden, R. Kremer, M. Lumsden, and H. Dabowska, *Phys. Rev. Lett.* **84**, 3446 (2000).
- [12] T. Barnes, J. Riera, and D. Tennant, *Phys. Rev. B* **59**, 11384 (1999).
- [13] H. von Schnering, Y. Grin, M. Kaupp, M. Somer, R. Kremer, O. Jepsen, T. Chatterji, and M. Weiden, *Z. Kristallographie – NCS* **213**, 246 (1998).
- [14] A. Meetsma, J. de Boer, A. damascelli, J. Jegoudez, A. Revcolevschi, and T. Palstra, *Acta Crystallogr. Sect. C* **54**, 1558 (1998).
- [15] H. Smolinski, C. Gros, W. Weber, U. Peuchert, G. Roth, M. Weiden, and C. Geibel, *Phys. Rev. Lett.* **80**, 5164 (1998).
- [16] T. Ohama, H. Yasuoka, M. Isobe, and Y. Ueda, *Phys. Rev. B* **59**, 3299 (1999).
- [17] J. Lüdecke, A. Jobst, S. van Smaalen, E. Morr e, C. Geibel, and H.-G. Krane, *Phys. Rev. Lett.* **82**, 3633 (1999).
- [18] J. de Boer, A. Meetsma, J. Baas, and T. Palstra, *Phys. Rev. Lett.* **84**, 3962 (2000).
- [19] A. Bernert, T. Chatterji, P. Thalmeier, and P. Fulde, *Euro. Phys. J. B* **21**, 535 (2001).
- [20] W. Schnelle, Y. Grin, and R. Kremer, *Phys. Rev. B* **59**, 73 (1999).
- [21] S. Bompadre, A. Hebard, V. Kotov, D. Hall, G. Maris, J. Baas, and T. Palstra, *Phys. Rev. B* **61**, R13321 (2000).
- [22] L. Bulaewskii, A. Buzdin, and D. Khomskii, *Sol. Stat. Comm.* **27**, 5 (1978).
- [23] P. Thalmeier and P. Fulde, *Europhys Lett.* **44**, 242 (1998).
- [24] D. Sa and C. Gros, *Euro. Phys. J. B* **18**, 421 (2000).
- [25] M. Mostovoy, J. Knoester, and D. Khomskii, *cond-mat/0009464* (2000).
- [26] A. Yaresko, V. Antonov, H. Eschrig, P. Thalmeier, and P. Fulde, *Phys. Rev. B* **62**, 15538 (2000).
- [27] P. Horsch and F. Mack, *Euro. Phys. J. B* **5**, 367 (1998).
- [28] A. Harris and R. Lange, *Phys. Rev.* **157**, 295 (1967).
- [29] P. Pfeuty, *Ann. Phys.* **57**, 79 (1970).
- [30] R. Houtappel, *Physica* **XVI**, 425 (1950).
- [31] J. Stephenson, *J. Math. Phys* **11**, 420 (1970).
- [32] A. Langari, M. Mart n-Delgado, and P. Thalmeier, *Phys. Rev. B* (2001).

- [33] E. Sherman, M. Fischer, P. van Lemmens, P. Loosdrecht, and G. Güntherodt, *Europhys. Lett.* **48**, 648 (1999).
- [34] V. Yushankhai and P. Thalmeier, *Phys. Rev. B* **63**, 4402 (2001).
- [35] M. Cross and D. Fisher, *Phys. Rev. B* **19**, 402 (1979).
- [36] U. Grenander and G. Szegő, *Toeplitz Forms and their Applications* (University of California Press, Berkeley and Los Angeles, 1958).
- [37] B. McCoy, *Phys. Rev.* **173**, 531 (1968).
- [38] H. Schwenk, S. Zherlitsyn, B. Lüthi, E. Morre, and C. Geibel, *Phys. Rev. B* **60**, 9194 (1999).
- [39] M. Cross, *Phys. Rev. B* **20**, 4606 (1979).
- [40] M. Dischner, C. Geibel, E. Morr e, and G. Sparn, preprint (2000).
- [41] M. Isobe and Y. Ueda, *J. All. Comp.* **262–263**, 180 (1997).
- [42] T. Ohama, A. Goto, T. Shimizu, E. N. H. Sawa, M. Isobe, and Y. Ueda, *J. Phys. Soc. Jpn.* **69**, 2751 (2000).
- [43] N. Suaud and M.-B. Lepetit, *Phys. Rev. B* **62**, 402 (2000).
- [44] P. Thalmeier and A. Yaresko, *Euro. Phys. J. B* **14**, 495 (2000).
- [45] S. Trebst and A. Sengupta, *Phys. Rev. B* **62**, R14613 (2000).
- [46] A. Honecker and W. Brenig, *cond-mat/0009298* (2000).
- [47] C. Gros, R. Valent ı, J. Alvarez, K. Hamacher, and W. Wenzel, *Phys. Rev. B* **62**, R14617 (2000).
- [48] B. Leuenberger, A. Stebler, H. G udel, A. Furrer, R. Feile, and J. Kjems, *Phys. Rev. B* **30**, 6300 (1984).
- [49] S. Haley and P. Erd os, *Phys. Rev. B* **5**, 1106 (1972).

TABLES

| | $\delta_{t_D} = \frac{t_{D+}-t_{D-}}{t_{D+}+t_{D-}}$ | δ_{t_L} | $\delta_J = \frac{J_+-J_-}{J_++J_+}$ |
|--|--|----------------|--------------------------------------|
| Na shift in c-direction | 0.0105 | -0.0135 | 0.0035 |
| V shift in b-direction | 0.0236 | 0.0136 | 0.0347 |
| Rung O shift in b-direction | 0.0072 | -0.0093 | -0.0016 |
| Rung O shift in b-direction with t_{OO} included | 0.102 | 0.003 | 0.096 |

TABLE I. Change of hopping matrix elements for an alternating Na shift in c-direction, an alternating V shift in b-direction and an alternating shift of rung O ions in b-direction respectively. Shift is by 1 pm per site on an otherwise undistorted ladder. The accompanying change of the superexchange has been calculated as the singlet-triplet gap on a cluster of two neighbouring rungs of a ladder [19].

FIGURES

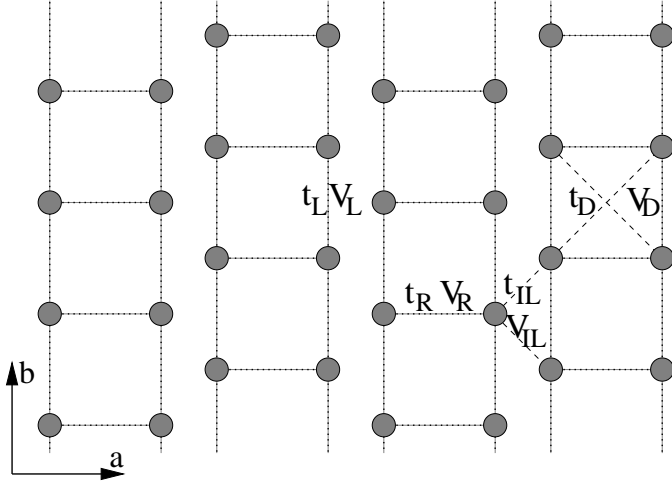


FIG. 1. Hopping matrix elements and Coulomb interactions in the V layers

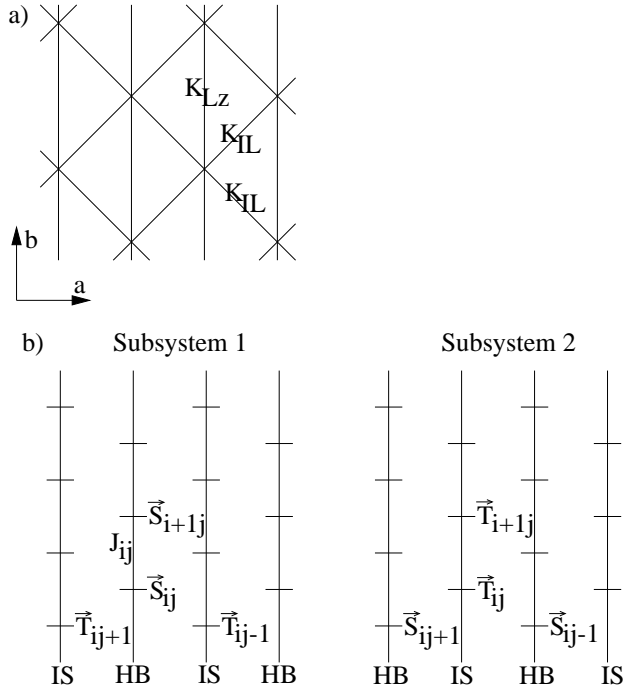


FIG. 2. a) Lattice geometry if one introduces \vec{S}_{ij} and \vec{T}_{ij} operators and represents each rung by a point. b) The two subsystems of the model described by (11) consisting of Ising (IS) pseudospin and Heisenberg (HB) spin chains.

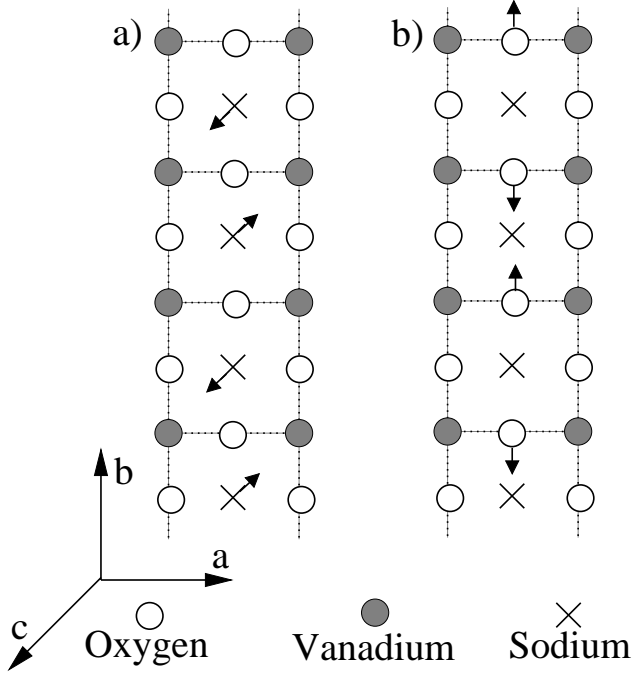


FIG. 3. a) Alternating Na shift in c -direction schematically shown by arrows causes superexchange alternation. b) Alternating shift of the rung O ions in b -direction causing superexchange alternation and inequivalence of the Na sites along the ladder.

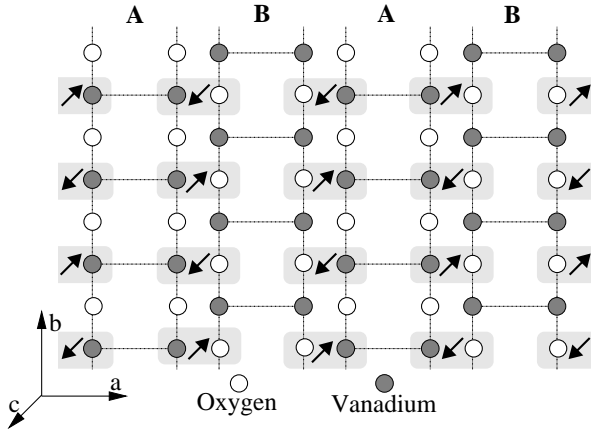


FIG. 4. The q_0 mode is shown, for which the V ion on one leg and O ion on neighbouring leg move together in c -direction as shown by arrows. This causes charge ordering on A ladders due to a staggered change of the V on-site energies and superexchange alternation on B ladders due to O ion motion. In experiment [19] shifts in a -direction are also observed which are not shown here.

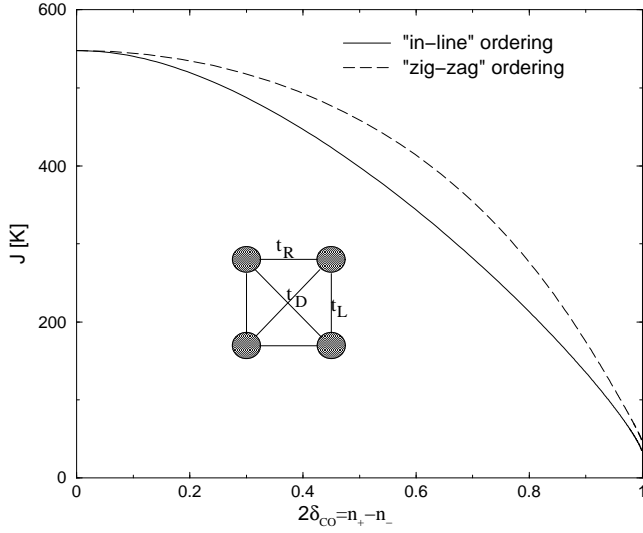


FIG. 5. Dependence of superexchange J on charge ordering. Results from cluster calculation for two rungs of the same ladder with parameters $t_R = 0.172$ eV, $t_L = 0.049$ eV, $t_D = 0.062$ eV, $V_L = 0.344$ eV, $V_R = 0.398$ eV, $U = 4$ eV and superexchange defined as the singlet-triplet gap [19]. “Zig-zag” charge ordering or “in-line” charge ordering was induced by changing the on-site energies with $\epsilon_1 = \epsilon_3 = -\epsilon_2 = -\epsilon_4$ for “in-line” ordering and $\epsilon_1 = -\epsilon_2 = -\epsilon_3 = \epsilon_4$ for “zig-zag” ordering. Inset shows geometry of cluster. The difference in the behaviour of the superexchange between the two ordering patterns comes from the fact that $t_L \neq t_D$ and $V_L \neq V_D = 0$.

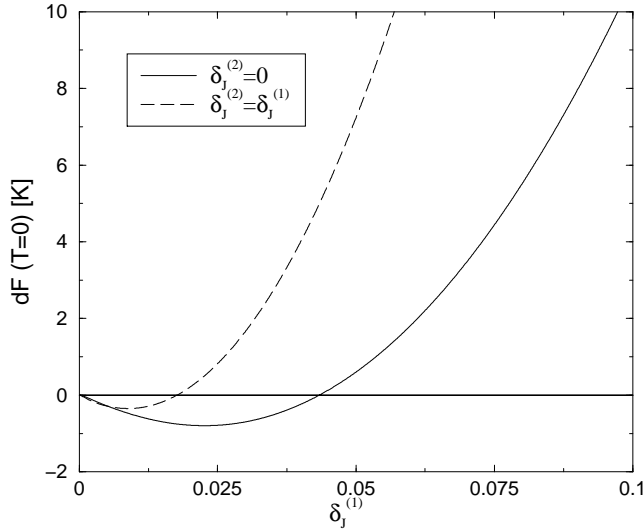


FIG. 6. Ground-state energy gain dF of the ordered system versus the disordered system depending on the order parameters.

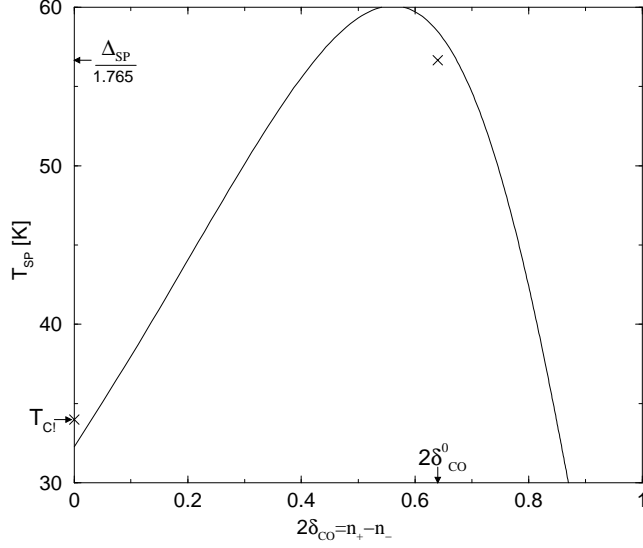


FIG. 7. T_{SP} -dependence on charge ordering for a spin-Peierls transition due to alternating shifts of the rung O ions on the A ladders in b direction. Dimerisation of hopping matrix elements for a shift of 1 pm given by $\delta_{t_D} = 0.090$ and $\delta_{t_L} = -0.059$. \times mark conditions (i) and (iii) (see text). The increase of T_{SP} for small δ_{CO} is due to increase of the effective δ_J resulting from increase of the hopping matrix elements due to the distortion accompanying the charge ordering. The decrease for large δ_{CO} is caused by the decrease of the average superexchange \bar{J} as shown in Fig. 5.

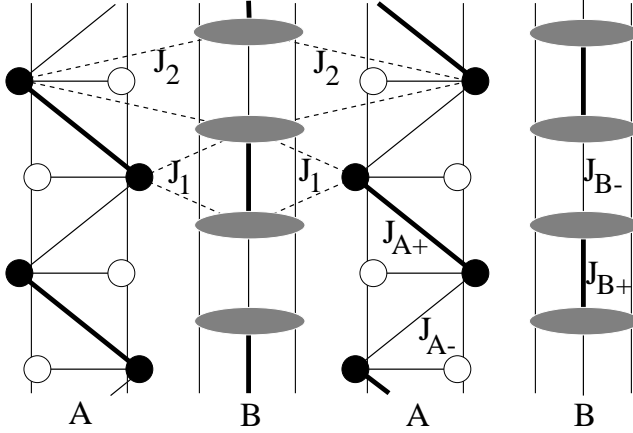


FIG. 8. Geometry of initial magnetic Hamiltonian (36). $J_{\pm} = J(1 \pm \delta)$ for the respective ladder.

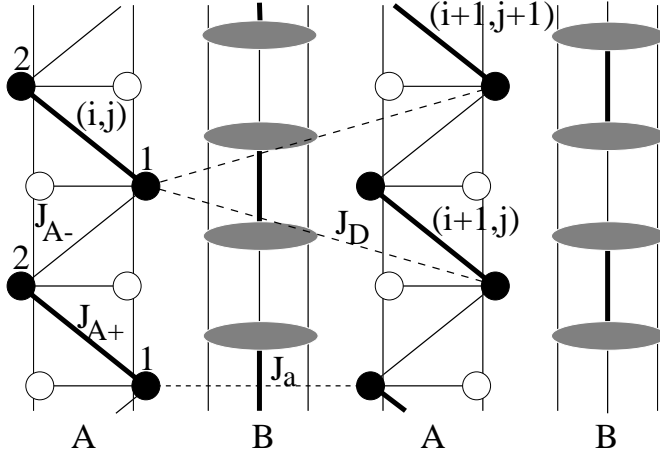


FIG. 9. Geometry of effective magnetic Hamiltonian (37). 1 and 2 denote the two spins of a dimer, J_a and J_D denote the effective superexchange between spins in the A ladder via the B ladder for nearest interladder neighbours and next-nearest interladder neighbours. V_{21} sites with increased electron density denoted by black circles, V_{22} sites with decreased electron density by white circles.

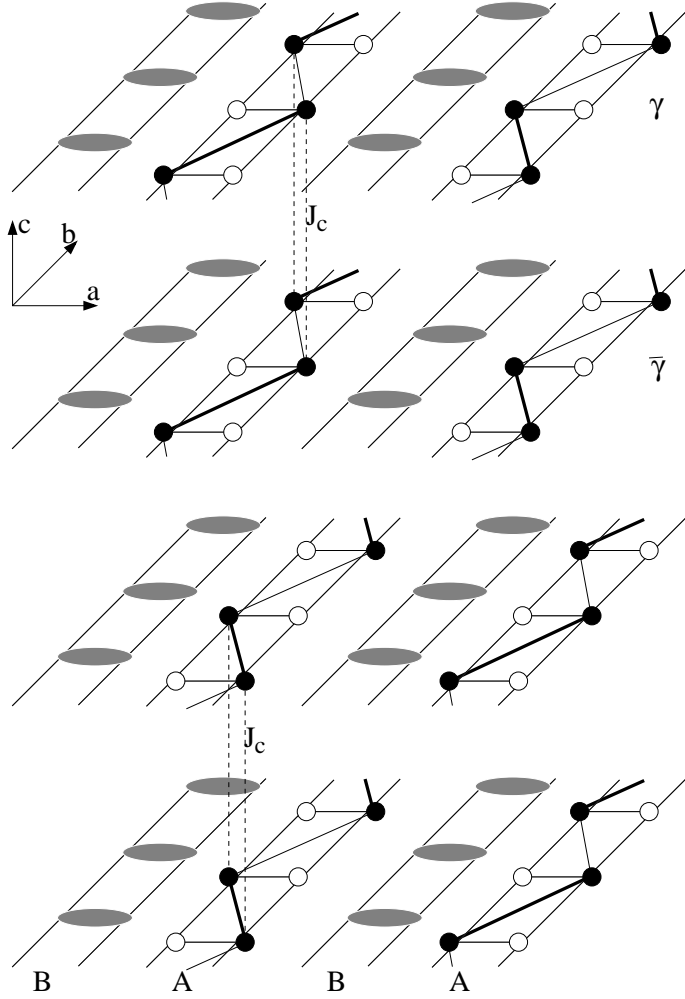


FIG. 10. Unit cell of low-temperature ordered state. Along the A ladders one has pairs of V_{21} sites (black circles) alternating with pairs of V_{22} sites (white circles) in c -direction. J_c therefore connects two layers $\gamma, \bar{\gamma}$ only. For such two layers, dimers on the A ladders are assumed to lie directly above each other in c -direction.

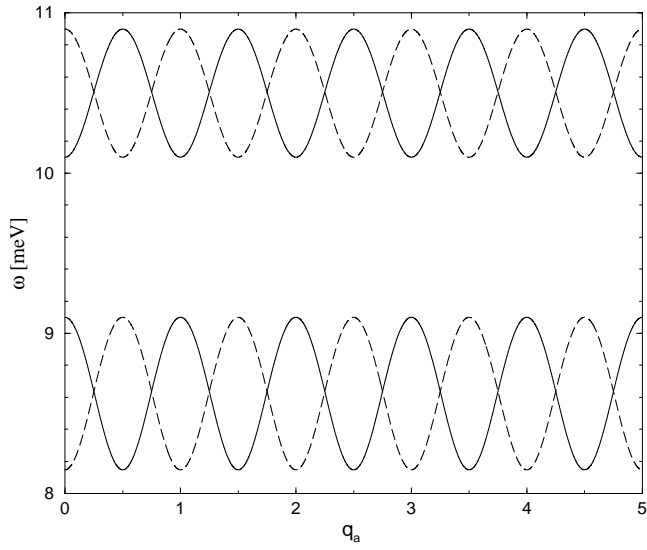


FIG. 11. Magnon dispersion along a-direction for $q_b = \frac{1}{2} = Q_b^{AF}$ (solid lines) and $q_b = 1 = Q_b^{ZC}$ (dashed lines).

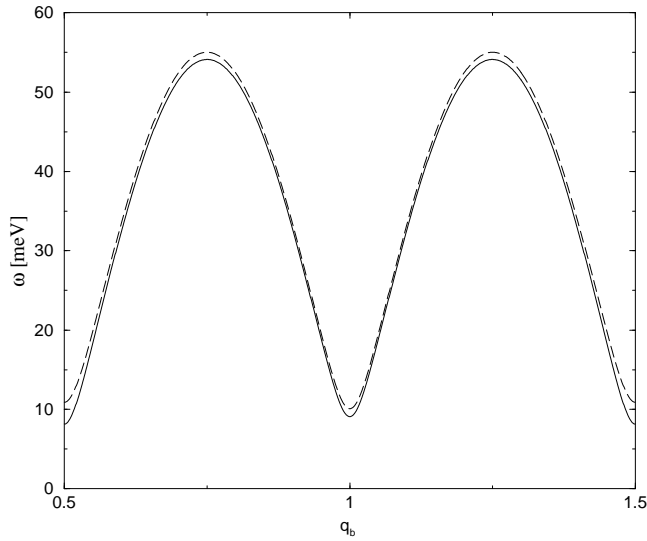


FIG. 12. Magnon dispersion along b-direction for $q_a = 3.5$.